Dolomite-zirconia reaction sintered bonded coarse magnesia ceramics: effect of the bonding proportion

F. Booth[1,2]*, F. M. Stabile[1,3], Y. Bruni[1,4], M. R. Gauna[1], N. M. Rendtorff[1,4]

[1]Centro de Tecnología de Recursos Minerales y Cerámica, CIC-CONICET La Plata, Camino Centenario y 506, C.C.49 (B1897ZCA) M.B. Gonnet, Buenos Aires, Argentina
[2]Universidad Nacional Del Chaco Austral, Chaco, Argentina
[3]Universidad Nacional de La Plata, Facultad de Ingeniería, Departamento de Ingeniería Química, Buenos Aires, Argentina
[4]Universidad Nacional de La Plata, Facultad de Ciencias Exactas, Departamento de Química, Buenos Aires, Argentina

Abstract

Refractory ceramic materials were manufactured, mainly composed of magnesia grains (coarse and medium fraction) and $CaZrO_3$/MgO as a binding phase produced from the reaction sintering between $CaMg(CO_3)_2$ (dolomite) and m-ZrO_2 (monoclinic zirconia), which constituted the finer fraction. Different relationships between the proportion and the size of the different aggregates were studied. The microstructure of the materials was characterized in terms of density, crystalline phases, grain phase distribution, and morphology. A combination of X-ray diffraction analysis and scanning electron microscopy with microanalysis was used. The mechanical behavior was determined in terms of the room temperature dynamic Young's modulus and the 3-point bending modulus of rupture (MOR) at room temperature. All the materials remained with porosities above 30%. The microstructure developed was similar between the sintered materials, characterized with MgO coarse grains bonded by $CaZrO_3$/c-ZrO_2 phases, and dispersed irregularly shaped pores. The MOR was directly related to the finer fraction content in the composition, where a higher quantity of finer fraction resulted in a higher MOR.
Keywords: magnesia, calcium zirconate, refractory ceramics.

INTRODUCTION

Refractory ceramics are designed to withstand different severe service conditions including high temperatures, corrosive liquids, and gases, abrasion, mechanical and thermal stresses. These are used in a wide range of industries, the most important being metallurgical, glass, and cement [1]. Particularly, cement is strategic and highly demanded by construction and public works. Currently, cement clinker production furnaces are used to incinerate polluting residues (rubber, organics of varied composition). Therefore, their resistance to the attack of corrosive agents from the waste products incinerated in these types of furnaces is an essential requirement for refractories [2]. In the synthesis of the cement clinker, limestone, clays, and other components that provide alumina and silica are used as raw materials. The reactions that take place among the raw materials in the clinkerization furnace are complex (mainly at 1450 °C) and actively involve the refractory lining that covers the interior of the kiln [3].

The development of refractory linings for cement kilns is closely linked to the processing of cement clinker in rotary kilns. In fact, in the 1920s, cement kilns were small and had an insignificant specific thermal load allowing silico-aluminous or high alumina bricks to be used even in hot areas. The development of more advanced technologies for cement production was accompanied by larger furnaces designed to withstand higher thermal loads, which required the development of new refractories capable of withstanding the increase of thermal loads. This requirement was partially addressed by introducing specific basic refractories based on magnesia with additional second-phases (SiO_2) [4, 5]. When magnesia (the main phase of these refractories) was added with different percentages of SiO_2 as a sintering additive, the phases obtained had a high coefficient of thermal expansion, and the resistance to spalling was low. The behavior of these materials at high temperatures depended on the content of the liquid phase and its distribution among solid phases. Therefore, the liquid phases tend to wet the periclase grains (MgO) creating a lubricating film between them that facilitates intergranular sliding resulting in deformation of the material at high temperatures. Adding chromium oxide to the periclase (greater than 15%) came as a partial solution for this problem. Thus, the first generation of spinel of chrome-magnesia refractories was developed. This modification in the composition of refractories significantly improved their characteristics, mainly the thermomechanical and physical abrasion, important properties required in service [6]. Although these materials exhibit acceptable behavior regarding thermomechanical requirements and

physical abrasion, they were strongly attacked by the cement clinker due to the incompatibility between the chrome spinel with the tricalcium silicate and lime that are part of the cement. The incompatibility of the clinker phases with the chrome spinel of the refractory allows these phases to react forming calcium chromite which, together with other phases present in the refractory that contain silica, form low melting compounds which facilitate the additional attack by chlorides, sulfates, and alkalis present in molten clinker [7]. The reaction of the chrome spinel present in the refractory with the silicates of the clinker under operating conditions produces a change in the chromium oxidation state from Cr^{3+} (non-toxic, non-carcinogenic, and insoluble) to Cr^{6+} (soluble and carcinogenic) [6, 8]. Currently, close attention is focused on the development of new chrome-free refractory materials that can resist not only the complex reactions triggered in the clinkerization process but also the chemical attacks generated by the components of the different alternative fuels used. Furthermore, the composition of the refractory and its microstructure are to be selected to allow raw material on the surface of the refractory to form a layer that covers and protects the material.

Coarse magnesia (MgO) ceramics are of technological interest. It is well known that the high covalence nature of this material is responsible for its difficulty in sintering at relatively low temperatures, ~1300 and 1400 °C, especially when the grain size is over 0.5 mm and lacks a lower content phase acting as a sintering agent that bonds large grains. Magnesia refractory materials, such as spinel, hercynite, and magnesioferrite, show good hot properties and have relatively high melting points to be used in the so-called hot zone of clinkerization furnaces at 1450 °C. These attractive properties were a key factor to their development together with a second-phase with a spinel structure throughout the last decade. It is widely known that the spinel structure in refractories of this type improves its thermomechanical properties [6, 8, 9]. An example of this is the magnesia/magnesia-spinel ($MgO/MgAl_2O_4$) refractories that show a marked difference in their coefficient of thermal expansion (α_{MgO}= 12.5 to 13.5 x10^{-6} °C^{-1} [10, 11]; $\alpha_{MgAl2O4}$=8.8x10^{-6} °C^{-1} [6]). This results in the formation of radial microcracks in the material during the cooling stage of the furnace. Microcracks dampen stresses and prevent them from spreading further by thermal shock. An excessive amount of spinel present in the material could generate a large number of microcracks resulting in a considerable reduction in the thermomechanical properties of the material [6, 12-15]. Hercynite and magnesioferrite are other components with the spinel structure that significantly improve the thermomechanical properties of periclase refractory materials, including thermal shock resistance. However, these refractories have not found extensive use in the cement industry. This is due to the high sensitivity of these spinels to oxidation under atmospheric conditions. In an oxidizing atmosphere, secondary spinel and a solid solution are formed in the material as a result of a change in the oxidation state of iron (Fe^{2+} to Fe^{3+}) that develops additional microcracks and a

reduction in the material mechanical resistance. In addition, materials that contain a relatively high amount of iron do not generally exhibit good resistance to the chemical attack generated by cement clinker [16].

Other chromium-free materials that are promising candidates for use in the hot zone of clinkerization furnaces and casting ladles for their excellent properties are those of the MgO-CaO-ZrO_2-SiO_2 system. Materials containing ZrO_2 are extensively used in the cement industry due to their properties. High melting point, good resistance to thermal shock, thermomechanical resistance, and mainly high resistance to clinker corrosion attack are some of the properties that make them potentially suitable for the manufacture of refractory bricks used in kilns in the cement industry. $CaZrO_3$ ceramics can be obtained efficiently through a reaction between m-ZrO_2 (monoclinic zirconia) and calcium-containing minerals such as calcite ($CaCO_3$) or dolomite [$MgCa(CO_3)_2$]; the stoichiometric reaction between zirconia and calcite forms $CaZrO_3$, but if the reaction is not stoichiometric, secondary phases such as c-ZrO_2 (cubic zirconia) can be formed. For the stoichiometric reaction between m-ZrO_2 and dolomite, the main phases formed are $CaZrO_3$/MgO. For both cases, the formation of second-phases such as c-ZrO_2, merwinite [$MgCa_3(SiO_4)_2$], monticellite ($CaMgSiO_4$), spinels, glasses, etc., is closely related to the impurity content of the mineral (SiO_2, Fe_2O_3, Al_2O_3) and play a key role in the properties of the material [17]. The greatest drawback presented by this attractive system is the relatively high-cost of m-ZrO_2 compared to other oxides. Therefore, the amount used should be limited to reduce the cost of the bricks and thus make their manufacturing profitable.

In this work, we show the results of the development of a refractory material formed mainly by coarse grains of MgO. These are bonded by a smaller proportion of $CaZrO_3$/MgO obtained by reactive sintering from an equimolar mixture of dolomite with submicron zirconia of high purity that constitutes the fine fraction and acts as a bonding phase. This phase acts as a binder between the larger magnesia grains, a finding studied in previous research whose results were encouraging to be used in refractories on a larger scale [17, 18].

MATERIALS AND METHODS

Starting powders and processing route: three types of ceramics were manufactured using commercial magnesite (MgO) grains (99 wt%, RHI, Brazil) bonded with equimolar mixtures of zirconia (ZirPro, Saint Gobain, China) and dolomite (DBZ); the employed natural dolomite and the other starting powders were fully described elsewhere [3]. The studied materials were called MDBZ1, MDBZ2, and MDBZ3. The processing route was equivalent and the granulometric distribution effect was studied. Mainly, the only difference was in the quantities of the medium and fine fractions (Table I). These compositions were selected for evaluating the influence of different sintering additive quantities (fine fraction) on the processing and properties of the final refractory material. This

study could help to determine the optimal quantity of sintering additives to take into account in the development of commercial refractory material. Coarse and medium fractions were constituted by magnesia grains and the fine fraction (matrix) was formed by the reactive DBZ mixture. Both employed magnesite fractions were characterized by X-ray diffraction (XRD), Rietveld quantitative phase analysis, and scanning electron microscopy (SEM); the fine fraction (DBZ) was characterized in previous works [17, 18]. Initially, grain sizes of coarse and medium fractions (MgO) were adjusted using a ball mill, and then they were screened using ASTM standard sieves in different fractions (Table I). Fig. 1 shows the particle size distribution curves of the individual fractions (coarse, medium and fine) used in the different ceramics (MDBZ1, MDBZ2, and MDBZ3). For the fine fraction, the D50 (median particle size) presented a value of 2.5 µm while for medium and coarse fractions the values were 120 and 500 µm, respectively. These powders were mixed with isopropyl alcohol in a planetary ball mill at 40 rpm for 12 h. Then the mixtures were dried in an oven at 60 °C for 24 h. Subsequently, specimens were obtained by uniaxial pressing at 50 MPa in the shape of bars of 60x10x5 mm. Finally, the thermal cycle used for all samples had a heating rate of 5 °C/min up to 1450 °C and holding time of 2 h at this temperature; this cycle was used in previous works [3, 17, 18].

Characterization methods: identification of crystalline

Table I - Compositions (wt%) of the starting mixtures.

Sample	MgO		Dolomite/ zirconia (1:1)
	Coarse fraction (-#20 +#25)	Medium fraction (-#25 +#100)	Fine fraction (-#100)
MDBZ1	40	35	25
MDBZ2	40	25	35
MDBZ3	40	10	50

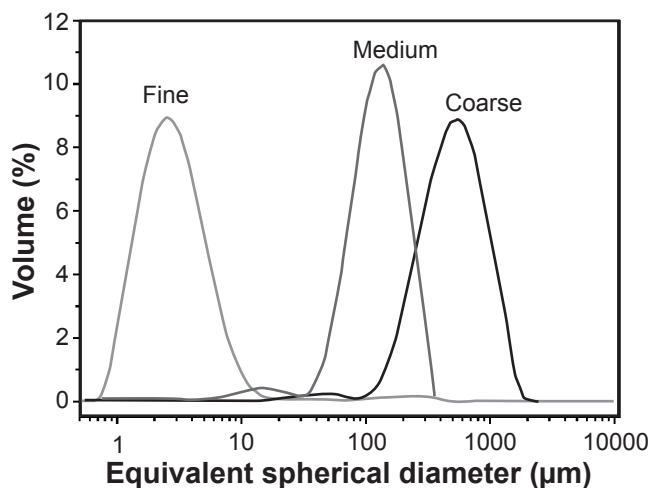*Notes: -#: passed through; +#: retained.*

Figure 1: Particle size distribution curves of the individual fractions (coarse, medium, and fine) used in the manufacture of three types of ceramics.

phases in the sintered ceramics was performed by X-ray diffraction (XRD) using a diffractometer (PW 3020/10, Philips) with CuKα radiation and Ni filter from 5° to 80° (2θ), a step of 0.04° and 2 s/step. The XRD patterns of raw materials were analyzed using the following ICCD PDF files: 36-0426 for dolomite [$CaMg(CO_3)_2$]; and 37-1484 for m-zirconia. For the sintered samples, the used files were: 35-0790 for calcium zirconate ($CaZrO_3$); 071-1176 for magnesia (MgO); 026-0341 for calcia-fully stabilized cubic zirconia (c-$Ca_{0.15}Zr_{0.85}O_{1.85}$); and 35-0591 for merwinite [Me: $Ca_3Mg(SiO_4)_2$]. The crystalline phase contents (wt%) of the materials were determined using the Rietveld method of refinement using the program FullProf v.2019 [19, 20]. The apparent density was measured by the Archimedes method using distilled water [3]. The relative density (D_r) of the sintered composite was calculated as the ratio between the apparent and theoretical density. Theoretical density was obtained using the rule of mixtures with values of density and volume fraction corresponding to each phase (determined based on Rietveld results). The total porosity was calculated as $P=1-D_r$. Microstructural characterization was performed on polished and C-coated specimens using a field emission scanning electron microscope, FE-SEM, with analysis by energy dispersive X-ray spectroscopy, EDX (Jeol, S-4700 I, Japan). The flexural strength or modulus of rupture (MOR) was measured on 10 samples by a 3-point bending test with a 40 mm span and a crosshead speed of 0.1 mm/min using a universal testing machine (5985, Instron, USA) [21]. The dynamic Young's modulus (E) for each composite was determined at room temperature by the impulse excitation technique (Grindosonic MK5 Industrial, Lemmens, Belgium) following the ASTM C1198 standard [22, 23]. The dynamic Young's modulus of the composite reported corresponded to the average of 5 measurements according to [24, 25]:

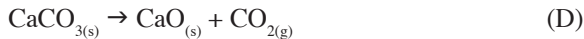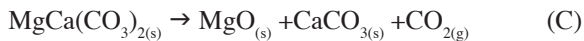$$E = 0.94642 \, \frac{\rho.l^4.f^2}{t^2} T \qquad\qquad (A)$$

where ϱ is the material's density, l is the length of the bar, f is the fundamental resonant frequency, t is the thickness of the beam, and T a correction factor given by Spinner and Tefft [24, 26]. The measured E values of the samples were low compared to the moduli at zero porosity (E_0), which were estimated taking into account the volumetric fraction (V_i) and the E_i modulus of each phase present from the phase rule. The equation that relates to these parameters is as follows:

$$E_{0,MDBZ}=E_{CaZrO3}.V_{CaZrO3}+E_{MgO}.V_{MgO}+E_{c-ZrO2}.V_{c-ZrO2}+E_{Me}.V_{Me} \quad (B)$$

RESULTS AND DISCUSSION

Crystalline phase composition determined by XRD using the Rietveld method: for all compositions (MDBZ1, MDBZ2, and MDBZ3), results of XRD, and the quantitative Rietveld phase analysis are summarized in Fig. 2 and Table II, respectively. R_{wp} values (Table II) indicated excellent fits

for refining. In all samples, the major phases were MgO and CaZrO$_3$, and c-ZrO$_2$ (Ca$_{0.15}$Zr$_{0.85}$O$_{1.85}$) and merwinite [Ca$_3$Mg(SiO$_4$)$_2$] were present in low amounts (<4 wt%), as minority phases; this was expected because the reaction between m-ZrO$_2$ and compound containing calcium and magnesium (dolomite) had been previously reported by a neutron diffraction study [27]. The reaction was shown to be sequential and the decomposition of dolomite occurred in two stages: the formation of MgO and CaCO$_3$ and subsequent decomposition of CaCO$_3$. Also, it was determined that MgO is formed directly without intermediate phases:

$$MgCa(CO_3)_{2(s)} \rightarrow MgO_{(s)} + CaCO_{3(s)} + CO_{2(g)} \qquad (C)$$

$$CaCO_{3(s)} \rightarrow CaO_{(s)} + CO_{2(g)} \qquad (D)$$

$$CaO_{(s)} + m\text{-}ZrO_{2(s)} \rightarrow CaZrO_{3(s)} \qquad (E)$$

The composition of the ceramic results from the global reaction:

$$MgCa(CO_3)_{2(s)} + m\text{-}ZrO_{2(s)} \rightarrow MgO_{(s)} + CaZrO_{3(s)} + 2CO_{2(g)} \qquad (F)$$

In the case of CaZrO$_3$ formation using pure dolomite, the kinetics follows a solid-state reaction model controlled by diffusion [27, 28]. In this way, the evolution of the phases formed in all ceramics (MDBZ1, MDBZ2, and MDBZ3) is associated with this mechanism. The contents of MgO and CaZrO$_3$ were different for each ceramic. This can be
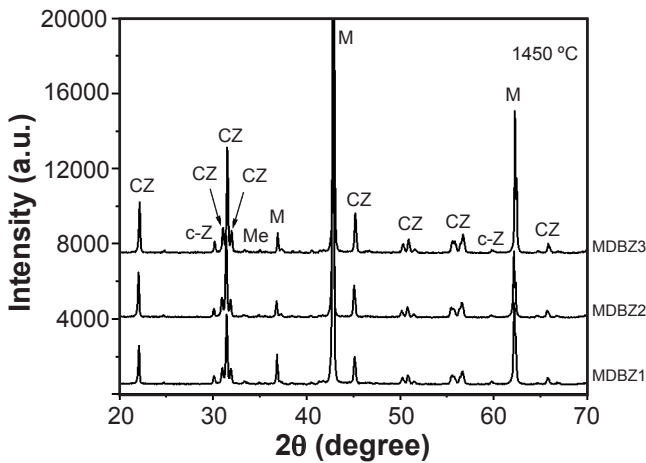
explained by the different compositions of the starting powders. However, in the minority phases, large variations were not determined for the different compositions studied. This could be due to the error in the quantification method.

Effect of processing variables on textural characteristics of MDBZ1, MDBZ2, and MDBZ3 composites: for all the composites, the achieved density was between 2.5 and 2.6 g/cm^3, and the linear shrinkage was low (around 5%), due to low densification (between 65% and 70% of the theoretical density). Thus, these materials exhibited relatively high porosity (between 30% and 35%). This could be improved by modulating more precisely the grain size distribution of the starting powders, for example introducing packing distributions proposed in [29], so as to achieve lower porosities, like commercial refractories, which are lower than 20%. However, the experimental design of this particular study was chosen in order to compare the effect of the change in the proportion of finer fraction (bonding additive) on the sintering properties of these materials of technological interest. Table III shows the results of total porosity, apparent, relative, and theoretical density for the composites studied.

Table III - Results of total porosity (P), apparent (D$_a$), relative (D$_r$), and theoretical (D$_t$) densities of sintered materials.

Sample	D$_a$ (g/cm^3)	D$_r$	D$_t$ (g/cm^3)	P (%)
MDBZ1	2.52	0.65	3.82	32
MDBZ2	2.56	0.65	3.89	35
MDBZ3	2.60	0.67	3.83	33

Mechanical properties of MDBZ1, MDBZ2, and MDBZ3 composites: the values of the elastic modulus corresponding to each phase in the different types of ceramic developed are shown in Table IV [3, 30]. The effect of porosity on modulus E can be estimated by an empirical model that predicts an exponential reduction of E with porosity [31-33]:

$$E = E_0 . e^{(-b.P)} \qquad (G)$$

For the typical configuration of a porous structure corresponding to the pore volume between sintered ceramic particles, the constant b is assumed to be 2.73 [31]. Table V shows the results of the modulus of elasticity at zero porosity (E$_0$) and those obtained from the employed model (Eq. G). As shown, the values of the experimental E are far from those predicted by the model (E$_M$). In fact, it was determined that the experimentally measured elastic moduli did not follow the rule of mixture. Therefore, the porosity effect cannot be satisfactorily represented by the Spriggs model. This could be attributed to the large number of pores that lack a defined shape [34], due to the fact that the models were build considering spherical pores. It is well known that finer powders have a higher sintering contraction than coarser powders [35]. The great contraction difference during sintering between the finer fraction and

Figure 2: XRD patterns for the studied materials MDBZ1, MDBZ2, and MDBZ3 sintered at 1450 °C/2 h. CZ: CaZrO$_3$, c-Z: Ca$_{0.15}$Zr$_{0.85}$O$_{1.85}$, M: MgO, Me: Ca$_3$Mg(SiO$_4$)$_2$.

Table II - Results of the Rietveld refinement for materials MDBZ sintered at 1450 °C for 2 h.

Sample	CaZrO$_3$	MgO	c-ZrO$_2$	Ca$_3$Mg(SiO$_4$)$_2$	R$_{wp}$
MDBZ1	15.25	81.95	0.99	1.81	18
MDBZ2	20.81	76.13	1.12	1.94	19
MDBZ3	24.25	71.57	1.18	2.76	19

the bigger magnesia grains could be the cause of the high porosity generated in all the materials. To overcome this, a continuous size distribution should be used, like those studied by Andreassen [29], so as to reach a better packing. Regarding the modulus of rupture (MOR), it was observed that an increase in the finer fraction content produced a higher MOR value. This behavior could be attributed to a higher intergranular bonding (coarse grains) as the sintering additive was increased, although the porosity remained on relatively high values. The sintered MDBZ3 composition reached a MOR value comparable to a typical commercial refractory [36-41].

Table IV - Young modulus, E (GPa), of the phases present in the sintered materials [3, 30].

$CaZrO_3$	MgO	$c-ZrO_2$	$Ca_3Mg(SiO_4)_2$
231	270	218	116

Table V - Results of flexural strength (MOR), Young's modulus (E), Young's modulus at zero porosity (E_0), and elastic modulus calculated from the empirical model as a function of porosity (E_M) of sintered materials.

Sample	MOR^a (MPa)	E^a (GPa)	E_0^b (GPa)	E_M^c (GPa)
MDBZ1	6.2 (±0.2)	11.3 (±2.0)	264.4	125
MDBZ2	9.0 (±1.0)	16.8 (±3.0)	260.0	113
MDBZ3	11.4 (±1.0)	20.0 (±2.0)	262.9	123

a: experimental; *b*: Eq. B; *c*: Eq. G.

Developed microstructure: the coarse magnesia microstructure was distinguished; Fig. 3 shows the microstructures of the 3 types of ceramic sintered at 1450 °C/2 h at low magnification. The SEM images show that the microstructures were mainly made up of a gray phase (grain of variable size: 20 to 500 μm) attributed to magnesia grains. In a smaller proportion, bordering the gray grains and dispersed throughout the microstructure, the second phase of white color was distinguished; this could correspond to the calcium zirconate. Finally, the third region of darker color was observed, throughout the microstructure of variable size and shape compatible with the continuous porosity of the studied materials. At higher magnification (Fig. 4), the light gray phase showed to contain small dark gray dots. This phase corresponded to the fine fraction of the ceramic named DBZ, whose composition, characteristics, and properties were described in previous work [17]. The SEM images showed that this gray color phase was found in a greater proportion in the MDBZ3 ceramic. The result was expected according to the formulations studied (Table I) indicating that it had the highest amount of DBZ fine fraction (50 wt%) formed by m-ZrO_2 (monoclinic zirconia) and $CaMg(CO_3)_2$ (dolomite) 1:1 molar ratio. In this case, phenomena of dolomite decarbonation, reaction, and sintering with m-ZrO_2 occurred
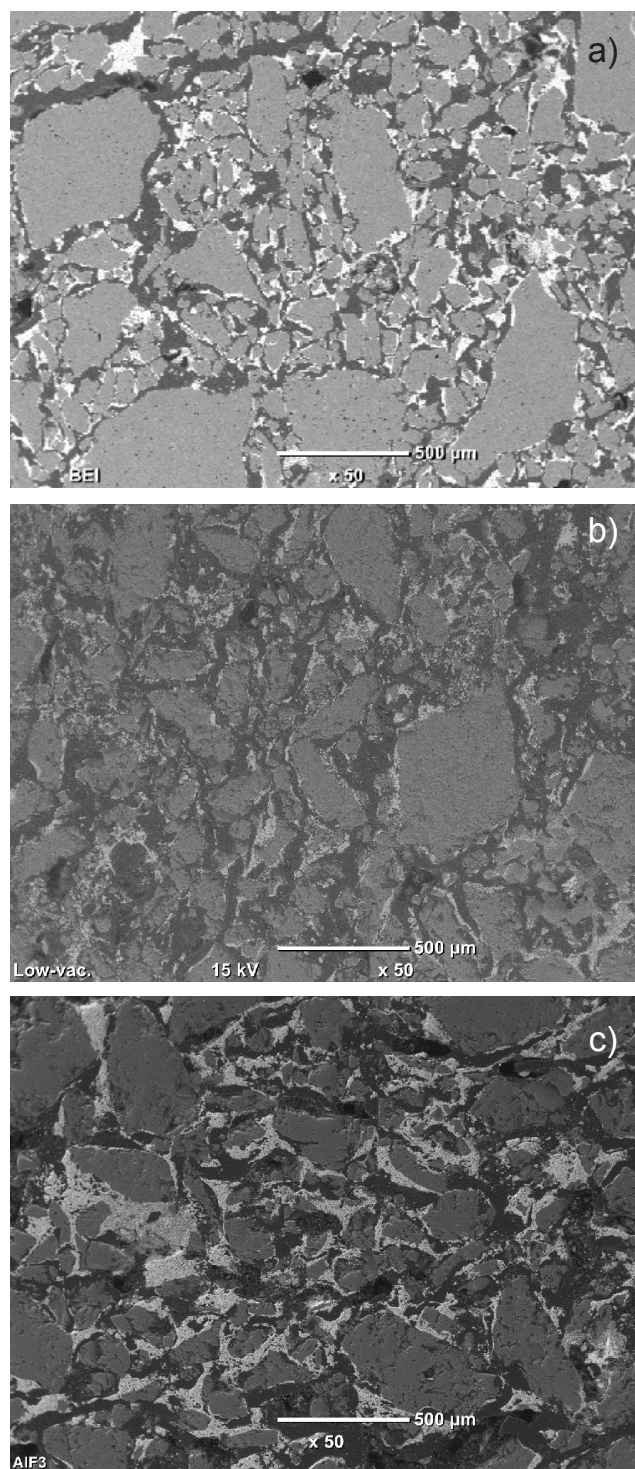

Figure 3: SEM images at a low magnification showing the microstructure of ceramics sintered at 1450 °C/2 h of: a) MDBZ1; b) MDBZ2; and c) MDBZ3.

to form $CaZrO_3$ and c-ZrO_2 during the heating stage, as previously reported [27].

The EDX analysis confirmed that the gray phase corresponded to MgO grains and the gray and white spots located on the grain border corresponded to the $CaZrO_3$/c-ZrO_2 phase. The dark color region corresponded to the composition of the resin infiltrated in the samples for the
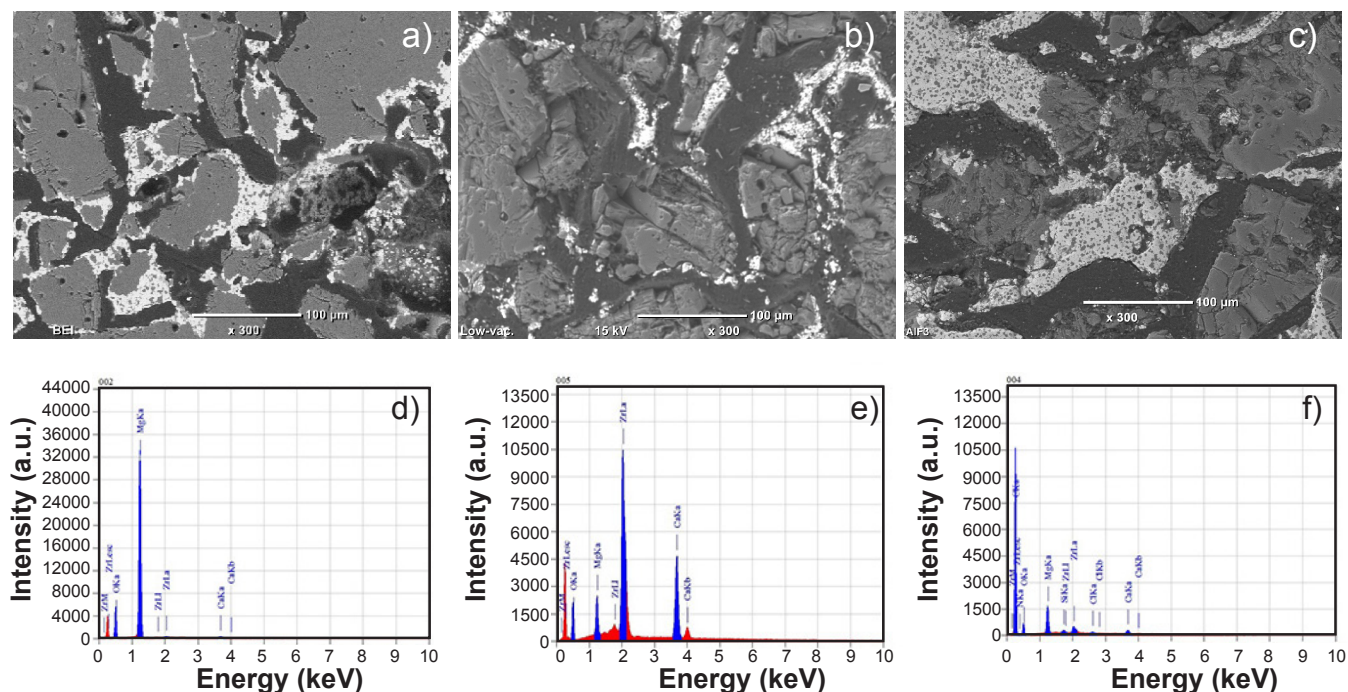
Figure 4: SEM images at a higher magnification showing the microstructure of ceramics sintered at 1450 °C/2 h of: a) MDBZ1; b) MDBZ2; c) MDBZ3; and EDX spectra of: d) gray phase (MgO); e) white phase (CaZrO$_3$); and f) dark-gray region (resin).

polishing stage, showing that it filled the open pores in the microstructure. The observed porosity was between 32% and 35% (Table III) and the pore structure was present in the three studied materials, showing the mentioned lack of packing of the coarse magnesia grains. Apparently, the pore channels were interconnected throughout the material. The observed pore diameter was below approximately 50 μm. Finally, some closed pores were observed within the magnesia grains, especially in the bigger coarse grains. From a detailed observation of SEM images, no cracks or loss of the microstructure integrity were observed within the magnesia grains and the calcium zirconate grains, showing a good reaction sintering process that ensured the consolidation of the ceramics.

CONCLUSIONS

Coarse magnesia (MgO) ceramics are of technological interest, especially for the cement industry. This type of material with a high content of MgO exhibits some difficulty to achieve sufficient bonding among grains as their optimum sintering temperature is over 1500 °C, especially if the grain size is relatively large and does not have a second bonding phase. Considering this fact, a new bonding strategy based on a zirconia dolomite reaction sintering was proposed and studied with firing at 1450 °C. No significant shrinkage was observed in the fired samples and the porosity remained relatively high (30%) in the studied composition range. The developed crystalline phases and microstructure features were described and the effect of the proportion of bonding starting powders was observed. The thermochemical processes were established as well. The ceramics showed

good mechanical properties. It was concluded that with the increase of fine fraction, the MOR (modulus of rupture) value increased, showing a better bonding effect, yet with higher raw materials cost. The developed ceramics fired at 1450 °C seem suitable for use as refractories in the cement manufacturing industry.

REFERENCES

[1] S.C. Caniglia, G.L. Barna, *Handbook of industrial refractories technology: principles, types, properties and applications*, Noyes Publ., New Jersey (1992) 23.
[2] J.L. Rodríguez, P.P. Castro, Bol. Soc. Esp. Ceram. V. **40**, 6 (2001) 463.
[3] R.F.N. Booth, "Procesamiento y caracterización de materiales cerámicos refractarios del sistema ZrO$_2$-CaO-MgO-SiO$_2$", Doct. Diss., Un. Nac. La Plata (2017).
[4] W.E. Lee, R.E. Moore, J. Am. Ceram. Soc. **81**, 6 (1998) 1385.
[5] C. Sadik, O. Moudden, A. El Bouari, I.E. El Amrani, J. Asian Ceram. Soc. **4**, 3 (2016) 219.
[6] J. Szczerba, E. Śnieżek, V. Antonovič, Refract. Ind. Ceram. **58**, 4 (2017) 426.
[7] P. Jiang, J. Chen, M. Yan, B. Li, J. Su, X. Hou, Int. J. Min. Met. Mater. **22**, 11 (2015) 1219.
[8] J. Szczerba, Cem. Lim. Gyp. **1990**, 4-5 (1990) 79
[9] J. Szczerba, J. Piech, Cem. Lim. Gyp. **1995**, 2 (1995) 57.
[10] M. Belmonte, Adv. Eng. Mat. **8**, 8 (2006) 693.
[11] Á. Obregón, J.L. Rodríguez-Galicia, J. López-Cuevas, P. Pena, C. Baudín, J. Eur. Ceram. Soc. **31**, 1-2 (2011) 61.
[12] R. Grasset-Bourdel, A. Alzina, M. Huger, D. Gruber, H. Harmuth, T. Chotard, J. Eur. Ceram. Soc. **32**, 5 (2012) 989.

[13] A. Ghosh, R. Sarkar, B. Mukherjee, S.K. Das, J. Eur. Ceram. Soc. **24**, 7 (2004) 2079.

[14] C. Aksel, P.D. Warren, F.L. Riley, J. Eur. Ceram. Soc. **24**, 8 (2004) 2407.

[15] C. Aksel, B. Rand, F.L. Riley, P.D. Warren, J. Eur. Ceram. Soc. **22**, 5 (2002) 745.

[16] M. Liu, Y. Li, S.L. Ma, W.B. Xia, Y.J. Li, Adv. Mat. Res. **476** (2012) 1523.

[17] F. Booth, L. Garrido, E. Aglietti, A. Silva, P. Pena, C. Baudín, J. Eur. Ceram. Soc. **36**, 10 (2016) 2611.

[18] A. Silva, F. Booth, L. Garrido, E. Aglietti, P. Pena, C. Baudín, Theor. Appl. Frac. Mech. **85** (2016) 125.

[19] H. Rietveld, J. App. Cryst. **2**, 2 (1969) 65.

[20] M.F. Hernández, P.V. López, A. Violini, G. Suárez, M.S. Conconi, N.M. Rendtorff, Sci. Sint. **51**, 4 (2019) 445.

[21] M.F. Serra, M.F. Acebedo, M.S. Conconi, G. Suarez, E.F. Aglietti, N.M. Rendtorff, Ceram. Int. **40**, 1 (2014) 1709.

[22] ASTM 1259-01, "Standard test method for dynamic Young's modulus, shear modulus and Poisson's ratio for advanced ceramics by impulse excitation of vibration", Am. Soc. Test. Mater. (2001).

[23] M. Musmeci, N.M. Rendtorff, L. Musante, L. Martorello, P. Galliano, E.F. Aglietti, Ceram. Int. **40**, 9 (2014) 14091.

[24] R.J.M. Toja, N.M. Rendtorff, E.F. Aglietti, T. Uchikoshi, Y. Sakka, G. Suárez, Ceram. Int. **44**, 12 (2018) 14348.

[25] G. Pickett, in Proc. ASTM **45** (1945) 846.

[26] S. Spinner, in Proc. ASTM **61** (1961) 1221.

[27] S. Serena, A. Caballero, M.A. Sainz, P. Convert, J. Campo, X. Turrillas, J. Am. Ceram. Soc. **87**, 9 (2004) 1706.

[28] J. Carretero, M.A. Sainz, S. Serena, A. Caballero, Bol. Soc. Esp. Ceram. V. **42**, 5 (2003) 303.

[29] Y.M. Chen, S.W. Doo, Powder Technol. **48**, 1 (1986) 23.

[30] Á. Obregón, J.L. Rodríguez-Galicia, J. López-Cuevas, P. Pena, C. Baudín, J. Eur. Ceram. Soc. **31**, 1-2 (2011) 61.

[31] R.M., Spriggs, J. Am. Ceram. Soc. **44**, 12 (1961) 628.

[32] R.M. Spriggs, L.A. Brissette, T. Vasilos, J. Am. Ceram. Soc. **45**, 8 (1962) 400.

[33] M. Higaeg, I. Balać, A. Grbović, M. Milovančević, M. Jelic, Sci. Sint. **51**, 4 (2019) 459.

[34] M.J. Vidal, T.S. Montolio, C. De la Fuente Cullell, Mater. Const. **51**, 261 (2001) 5.

[35] A.G. King, *Ceramic technology and processing: a practical working guide*, William Andrew (2001).

[36] J. Jakić, G. Štefanić, M. Labor, V. Martinac, Sci. Sint. **49**, 1 (2017) 61.

[37] J. Liu, X. Lv, J. Li, X. Zeng, Z. Xu, H. Zhang, L. Jiang, Sci. Sint. **48**, 3 (2016).

[38] C. Aksel, B. Rand, F.L. Riley, P.D. Warren, J. Eur. Ceram. Soc. **22**, 5 (2002) 745.

[39] A.G.M. Othman, N.M. Khalil, Ceram. Int. **31**, 8 (2005) 1117.

[40] J.E. Contreras, G.A. Castillo, E.A. Rodríguez, T.K. Das, A.M. Guzman, Mater. Charact. **54**, 4-5 (2005) 354.

[41] A. Ghosh, R. Sarkar, B. Mukherjee, S.K. Das, J. Eur. Ceram. Soc. **24**, 7 (2004) 2079.